



Cite this: *Energy Adv.*, 2025,  
4, 1375

Received 19th June 2025,  
Accepted 2nd October 2025

DOI: 10.1039/d5ya00163c

rsc.li/energy-advances

## The hydrolysis properties of polyethylene glycol under ambient nonthermal plasma conditions

Parsa Pishva,<sup>a</sup> Abdol Hadi Mokarizadeh,<sup>b</sup> Rongxuan Xie,<sup>a</sup> Jinyao Tang,<sup>ib</sup>  
Xiaochen Shen,<sup>a</sup> Yanlin Zhu,<sup>a</sup> Mesfin Tsige<sup>ib</sup>\*<sup>b</sup> and Zhenmeng Peng<sup>ib</sup>\*<sup>a</sup>

Polyethylene glycol (PEG) has been widely used in various industries for its biodegradability. However, the biodegradation of high molecular weight PEGs poses challenges due to limited microbial uptake. In this study, we investigated a rapid nonthermal plasma-assisted hydrolysis method to break down long-chain PEGs into shorter chains and valuable liquid and gas products. Utilizing a dielectric barrier discharge (DBD) reactor under ambient conditions, we achieve complete conversion of PEG into gas and liquid products, including methane (CH<sub>4</sub>), carbon monoxide (CO), carbon dioxide (CO<sub>2</sub>), methanol (CH<sub>3</sub>OH), ethanol (C<sub>2</sub>H<sub>5</sub>OH), acetic acid (CH<sub>3</sub>COOH), and ethylene glycol (C<sub>2</sub>H<sub>6</sub>O<sub>2</sub>), in mere minutes, which is significantly faster than conventional hydrolysis and biodegradation methods. Experimental results show that liquid products dominate throughout the reaction, while gas products increase over time, arising from secondary reactions of the liquid intermediates. Density functional theory (DFT) calculations elucidate the reaction pathways responsible for product generation. These findings highlight the promise of nonthermal plasma-assisted hydrolysis as an efficient approach for converting PEG into short-chain products and valuable chemical intermediates.

## Introduction

Polyethylene glycol (PEG) which is an organic water-soluble polymer with a structure represented as H(OCH<sub>2</sub>CH<sub>2</sub>)<sub>n</sub>OH has diverse applications in various industries, including the production of cosmetics, water-soluble lubricants, antifreeze agents, surfactants, plastics, and pharmaceutical preparations. It has been well documented that PEG undergoes biodegradation in the presence of bacteria, whether in aerobic or anaerobic conditions, achieved by the cleavage of ether bonds.<sup>1–3</sup> However, the process of PEG biodegradation under either aerobic or anaerobic conditions reveals that the growth potential of bacterial strains is influenced by the molecular weight ( $M_w$ ) and structural conformation of PEG molecules.<sup>3,4</sup> It has been reported that the biological oxidation of PEG is inherently very slow and becomes even slower as the polymer chain length increases. This reduction continues until the polymer molecules reach a size where they cannot enter the cell, preventing degradation.<sup>1,5</sup> For instance, certain studies indicate that PEGs with a molecular weight exceeding 1000 are not biodegradable.<sup>5</sup> It has also been reported that various factors, including water content, pH, temperature, UV light exposure, the presence of enzymes, oxygen, and oxidants like reactive oxygen species (ROS), significantly influence the

biodegradability of PEG. As a result, PEG cannot be universally classified as biodegradable under all environmental conditions.<sup>6</sup> Therefore, developing a method to efficiently decompose PEG of any chain length within a short reaction time is essential.

On the other hand, while PEG is typically regarded as nearly non-toxic, researchers have identified certain safety concerns related to both low and high molecular weight PEG.<sup>7</sup> Smyth *et al.* documented chronic oral toxicity of PEG oligomer ( $M_n \sim 200$ ) in rats, revealing adverse effects that were also observed in monkeys.<sup>8,9</sup> Liu *et al.* also confirmed that PEG-1000 and PEG-4000 show moderate cytotoxicity, especially at high concentrations. This implies potential safety issues with these seemingly safe materials.<sup>7</sup> Moreover, it has been reported that each PEG must be individually tested for biological effects, as these cannot be reliably predicted based solely on average molecular weight. PEGs with varying molecular weights may exhibit different levels of toxicity, highlighting the need for comprehensive testing.<sup>10</sup> Hence, finding effective methods for the decomposition of PEG becomes crucial, particularly in situations where biodegradation is not possible.

Some researchers have explored thermal methods for the decomposition of PEG, but employing this approach requires a long time for the decomposition of PEG, especially the ones with high molecular weight. For example, Han *et al.* showed that the thermal degradation of PEG, with a molecular weight of 6000, at 80 °C, requires 1000 hours of reaction.<sup>11</sup> Glastrup *et al.* showed that the thermal decomposition of tetraethylene glycol (TEG), utilized as a model molecule for PEG, at 70 °C for

<sup>a</sup> Department of Chemical Engineering, University of South Carolina, Columbia, South Carolina 29208, USA. E-mail: zmpeng@sc.edu

<sup>b</sup> Department of Polymer Science, The University of Akron, Akron, Ohio, 44325, USA

one week, can only result in the decomposition of 80% and 75% of the TEG under dry and humid conditions, respectively.<sup>12</sup>

The unique chemistry and high reactivity of nonthermal (non-equilibrium) plasma present significant potential for overcoming kinetic and thermodynamic barriers in polymer upcycling.<sup>13–15</sup> Compared to thermal plasmas, nonthermal plasma is more advantageous due to its lower energy requirements and reduced equipment costs.<sup>16,17</sup> Several types of nonthermal plasmas are utilized, including glow discharge (GD), microwave discharge (MD), corona discharge (CD), and dielectric barrier discharge (DBD). GD enables uniform surface modifications and effective oxidation of materials, while MD stands out for its high energy efficiency, allowing rapid production of materials with varied properties. DBD, recognized for its versatility, can function at both atmospheric and sub-atmospheric pressures.<sup>18–21</sup> DBDs are specialized electrode-based plasma reactors, primarily designed for low-temperature processing at atmospheric pressure. They consist of two electrodes—one high-voltage and one grounded—separated by at least one dielectric material.<sup>18,22</sup> While GD, MD, and DBD plasmas achieve higher polymer conversion rates than CD, challenges such as low energy efficiency and coke formation remain. However, DBD-based reactions offer significant advantages over conventional methods, including faster reactions and the elimination of the need for high pressures or extreme temperatures typically required in hydrolysis reactions.<sup>23</sup> Furthermore, DBD reactors, which operate at atmospheric pressure, simplify the process and enable continuous processing, distinguishing them from low-pressure nonthermal plasmas.<sup>16,24,25</sup>

Therefore, in this study, we explore a novel strategy that utilizes nonthermal plasma in a dielectric barrier discharge (DBD) tubular reactor to enable the efficient nonthermal plasma-assisted decomposition of PEG in the presence of water vapor under ambient temperature and pressure conditions and investigate the effect of reaction time on the PEG conversion and yield of different products. The nonthermal plasma can produce highly reactive species from water vapor, mainly in the form of ions and radicals. These species play a crucial role in breaking the bonds within the PEG structure, resulting in a very fast reaction that can facilitate PEG decomposition compared to conventional thermal methods. On the other hand, unlike the mentioned thermal-based methods, nonthermal plasma-assisted decomposition in the presence of water vapor does not require high temperatures for efficient bond cleavage in PEG. Moreover, this method significantly reduces the probability of contamination or the addition of impurities to the final products of the reaction. Finally, to the best of our knowledge, a thorough investigation of the products resulting from the decomposition of PEG has not been undertaken; therefore, the present study thoroughly investigates all products obtained from nonthermal plasma-assisted decomposition of PEG in the presence of water vapor.

## Experimental

### Materials

PEG (Sigma-Aldrich, Germany) powder was used for the non-thermal plasma-assisted hydrolysis reaction. Quartz wool

(Thermo Fisher Scientific, UK) was used to fix the PEG pellets inside the DBD reactor. Ar (99.999%) gas was purchased from Airgas. After the hydrolysis reaction, deuterium oxide (D<sub>2</sub>O) (99.9%, Cambridge Isotope Laboratories, Inc., USA) was used as the solvent to prepare the samples for the nuclear magnetic resonance (NMR) spectroscopy, and 2,5-dihydroxybenzoic acid (Bruker, Germany) and acetonitrile (99.9%, Sigma-Aldrich, USA) were used as the matrix and solvent, respectively, to prepare the samples for the matrix-assisted laser desorption/ionization-time of flight (MALDI-TOF) mass spectrometry.

### Plasma-assisted hydrolysis of PEG

Plasma-assisted hydrolysis experiments were carried out using a quartz tube reactor (ID: 13 mm) equipped with a dielectric barrier discharge (DBD) plasma generator to assist in the hydrolysis of PEG through nonthermal plasma. Non-thermal plasma was generated in the plasma generation zone (Fig. 1) within the reactor. The volume of the plasma zone was approximately 4 cm<sup>3</sup>. For each experiment, 1 g PEG pellets with a size of 125–250 μm were placed inside the DBD reactor. A flow of argon at a rate of 100 ml min<sup>−1</sup> was employed to pass through deionized (DI) water contained within a fully sealed container. This process generated water vapor, which then directly entered the plasma region to generate the active species necessary for the hydrolysis of PEG. The power input utilized in all experiments in this study was 25 W. To investigate the effects of reaction time on the reaction properties, 7 different reaction times (2, 5, 10, 15, 20, 30, and 40 minutes) were employed.

The weight reduction method was primarily employed to measure the mass of the gas product. The liquid product was extracted from the DBD reactor and weighed immediately after the hydrolysis reaction. In case solid, unreacted PEG remained at the end of the hydrolysis reaction, the weight of the solid unreacted PEG was found by computing the difference between the weight of the quartz wool and the solid residues.

The conversion (*X*, %) and product distribution (*Y*, wt%) were calculated by the following equations:

$$X = \frac{m_P - m_{RP}}{m_P} \times 100 \quad (1)$$

$$Y = \frac{m_{\text{gas}}/m_{\text{liquid}}/m_{\text{solid}}}{m_P} \times 100 \quad (2)$$

where *m<sub>P</sub>*, *m<sub>RP</sub>*, *m<sub>gas</sub>*, *m<sub>liquid</sub>*, and *m<sub>solid</sub>*, represent the mass of PEG, residual PEG, gas product, liquid product, and solid residue, respectively. To identify high-energy plasma species of water vapor nonthermal plasma, optical emission spectroscopy (OES, Ocean Optics USB4000 with fiber optic cable) was employed.

### Product analysis and characterization

As shown in Fig. 1, the end of the DBD tubular reactor, wherein the PEG hydrolysis reaction takes place, was connected to an online Universal Gas Analyzer 300 to analyze and quantify the gas products as they are produced. The gas products were also analyzed by *in situ* Fourier transform infrared (FTIR) spectroscopy



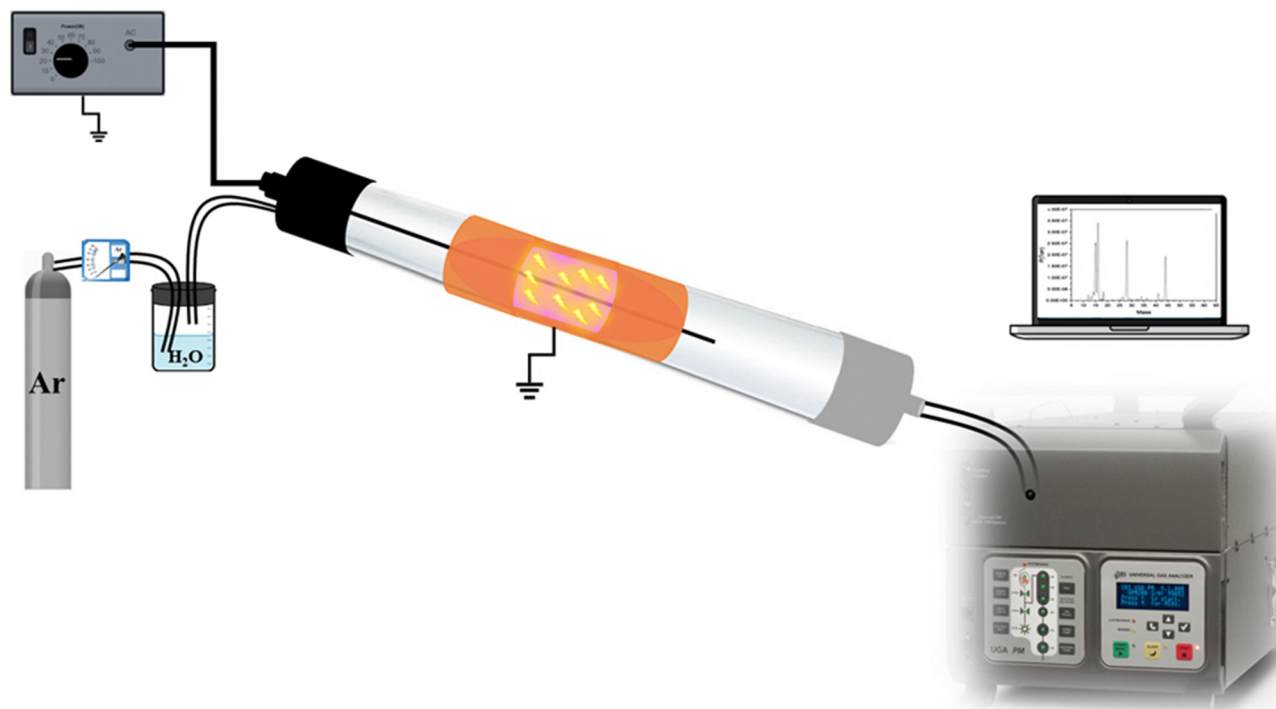


Fig. 1 Schematic of the DBD reactor system for nonthermal plasma-assisted hydrolysis of PEG.

with Nicolet 6700 IR spectrometer to confirm data obtained from the gas analyzer during plasma-assisted hydrolysis of PEG.

PEG and liquid products after plasma-assisted hydrolysis reaction were analyzed by proton nuclear magnetic resonance ( $^1\text{H-NMR}$ ) using Bruker Avance III-HD 400 MHz. For this purpose, liquid products were dissolved in  $\text{D}_2\text{O}$  with a  $10 \text{ mg ml}^{-1}$  concentration. Next, liquid products were characterized with matrix-assisted laser desorption/ionization time-of-flight mass spectroscopy (MALDI-TOF) using a Bruker Ultraflex II MALDI-TOF/TOF instrument. Both liquid products and 2,5-dihydroxybenzoic acid, which was used as the matrix, were dissolved in acetonitrile with concentrations of  $0.5 \text{ mg ml}^{-1}$  and  $5 \text{ mg ml}^{-1}$ , respectively.  $0.5 \mu\text{l}$  of liquid solution and  $0.5 \mu\text{l}$  of matrix solution were dropped onto the sample plate spot and dried in air at room temperature. Positive ion MALDI-TOF MS spectra of bio-oil samples were recorded with reflectron detection mode. Accelerating voltage, laser intensity, and overall laser shots were 20 kV, 50%, and 5000, respectively. The detection range was between 500–10 000 Da.

## Results and discussion

### Product distribution of PEG hydrolysis

The non-thermal plasma-assisted hydrolysis of PEG yielded gas and liquid products. Fig. 2 illustrates the influence of reaction time on the yield of these products. According to Fig. 2, it is evident that all reaction times resulted in the conversion of whole PEG into liquid and gas products, except for the 2-minute reaction for which 11% of the PEG remained unreacted at the end of the reaction. These results confirm

that the non-thermal plasma method is significantly faster compared to conventional thermal methods for the hydrolysis of PEG. A longer reaction time results in a slight reduction in the production of liquid products, accompanied by a small increase in the production of gas products. This suggests that prolonging reaction time results in the initiation of secondary reactions within the initially produced liquid products during the hydrolysis reaction, facilitating their conversion into gaseous products by the cleavage of various chemical bonds within their structures, as will be discussed later. However, it should

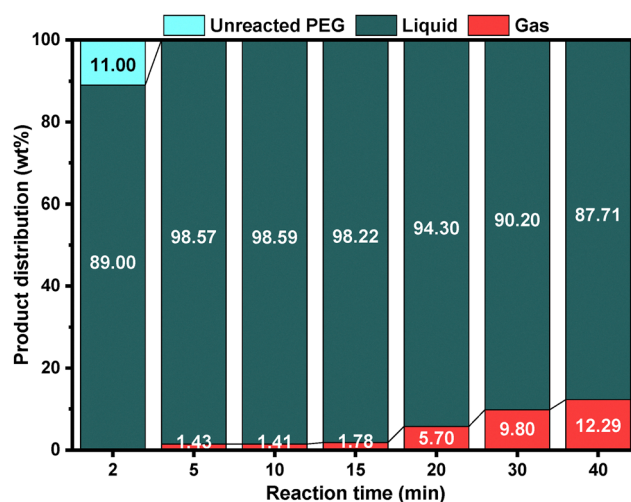


Fig. 2 The effect of reaction time on the distribution of gaseous and liquid products in nonthermal plasma-assisted hydrolysis of PEG (input power = 25 W).



be noted that increasing the reaction time from 5 to 40 minutes results in an increase in specific energy consumption, decreasing the energy efficiency from 2.08 to 16.67 kWh kg<sup>-1</sup>. This is close to the energy efficiency observed in our latest study on nonthermal plasma-assisted hydrogenolysis of lignin, where the highest energy efficiency was around 13 kWh kg<sup>-1</sup>.<sup>26</sup> However, due to the short reaction time and low input power used in our current research, the energy efficiency is significantly higher than in some other studies. For example, our previous study on nonthermal plasma-assisted hydrogenolysis of polyethylene demonstrated an energy consumption of 4000 kWh kg<sup>-1</sup> (0.25 g kWh<sup>-1</sup>) at an input power of 60 W.<sup>13</sup> Liu *et al.* also utilized a DBD reactor to decompose toluene, serving as a model compound for biomass tar. Their catalytic reaction, conducted at an input power of 35 W, achieved an energy efficiency of 385 kWh kg<sup>-1</sup> (2.6 g kWh<sup>-1</sup>).<sup>27</sup>

### Effect of reaction time on the gas products

The gas products, which are the minor products, were analyzed in real-time during the hydrogenolysis reaction using a gas analyzer (Fig. S1), and for result verification, they were reanalyzed once again using FTIR (Fig. S2). As can be seen in Fig. S1 and S2, the main gas products include methane (CH<sub>4</sub>), carbon monoxide (CO), and carbon dioxide (CO<sub>2</sub>). Furthermore, with an increase in reaction time, the weight percentage of all gas products increased, with CH<sub>4</sub> and CO showing the most substantial increase (Fig. 3).

As will be shown later, the formation of ethanol, methanol, and acetic acid during hydrolysis of PEG plays a crucial role in the formation of gas products. Methanol and ethanol can react with hydroxyl radicals generated from water vapor plasma to yield formaldehyde and acetaldehyde, respectively, which can subsequently react with hydroxyl radicals to produce CH<sub>4</sub>, CO, and CO<sub>2</sub>, as will be discussed later.

### Effect of reaction time on the liquid products

As shown in Fig. 2, the major PEG hydrolysis products are liquid. Therefore, the <sup>1</sup>H NMR and MALDI analyses were employed to analyze liquid products. According to Fig. 4, the <sup>1</sup>H NMR spectrum of PEG displays a broad triplet peak at approximately 3.6–3.7 ppm, attributed to the methylene protons (–OCH<sub>2</sub>) within the PEG structure.<sup>28–31</sup> Considering the structural similarity between ethylene glycol and PEG, which is formed from ethylene glycol units, their <sup>1</sup>H NMR peaks may overlap if ethylene glycol forms during hydrolysis of PEG.<sup>32</sup>

After the hydrolysis reaction, the <sup>1</sup>H NMR spectra of liquid products show distinct changes. Following a 10-minute reaction time, a new triplet peak emerges at 1.12 ppm, attributed to the methyl (–CH<sub>3</sub>) group of ethanol, and becomes more significant after 15 minutes of the hydrolysis reaction.<sup>33</sup> The methylene group (–CH<sub>2</sub>) of ethanol typically resonates at around 3.6 ppm, which overlaps with the broad –OCH<sub>2</sub> peak of PEG. It should be noted that, due to the use of D<sub>2</sub>O as the NMR solvent, peaks associated with hydroxyl (–OH) functional groups are absent, as they equilibrate with D<sub>2</sub>O to form R-OD and H<sub>2</sub>O.<sup>34</sup>

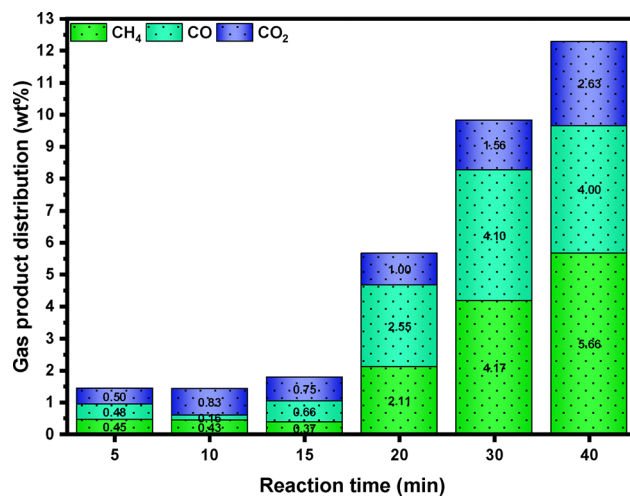


Fig. 3 The effect of reaction time on the distribution of different gas products of noncatalytic nonthermal plasma-assisted hydrolysis of PEG.

Moreover, after 10 minutes of hydrolysis, two singlet peaks appear at 2.16 and 3.31 ppm, indicating the presence of acetic acid and methanol, respectively.<sup>35–37</sup> Therefore, according to the <sup>1</sup>H NMR analysis, the main liquid products resulting from a 5-minute or longer hydrolysis reaction time include ethanol, methanol, and ethylene glycol. All identified liquid products are well-established industrial chemicals with broad utilization pathways. In principle, conventional separation and purification methods such as fractional distillation, membrane separation, or solvent extraction could be applied to recover these compounds from the reaction mixture.<sup>38</sup> Methanol and ethanol may serve as renewable fuels or blending agents,<sup>39</sup> acetic acid is widely used as a precursor in polymer and chemical synthesis,<sup>40</sup> and ethylene glycol has applications in antifreeze formulations and polyester production.<sup>41</sup> While detailed techno-economic analysis and process integration are beyond the scope of this study, these pathways highlight the potential practical relevance and industrial applicability of plasma-assisted PEG conversion. The reaction pathway leading to these products will be thoroughly discussed in the subsequent section.

Fig. 5 shows the MALDI analysis of the PEG and samples after the hydrolysis reaction. Due to the presence of long chains with different lengths in the PEG and its liquid products, the MALDI spectra show several peaks representing the distribution of the mass related to those chains. Based on these results, the peak of mass distribution related to the PEG is located around the *m/z* value of 2000. After 2 minutes of the hydrolysis reaction, the *m/z* distribution peak shifted slightly to lower values, while after 5 minutes or longer reaction times, the peak shift was more significant, confirming the effective bond cleavage in the PEG and formation of shorter chains due to the non-thermal plasma assisted hydrolysis reaction. The formation of new shorter chains continues and the *m/z* value reaches 950 after 40 minutes of reaction, which is less than half of the value related to the unreacted PEG. Moreover, a notable observation is the narrowing of the peak representing the mass distribution of PEG. This indicates that with increased reaction time, more bonds within





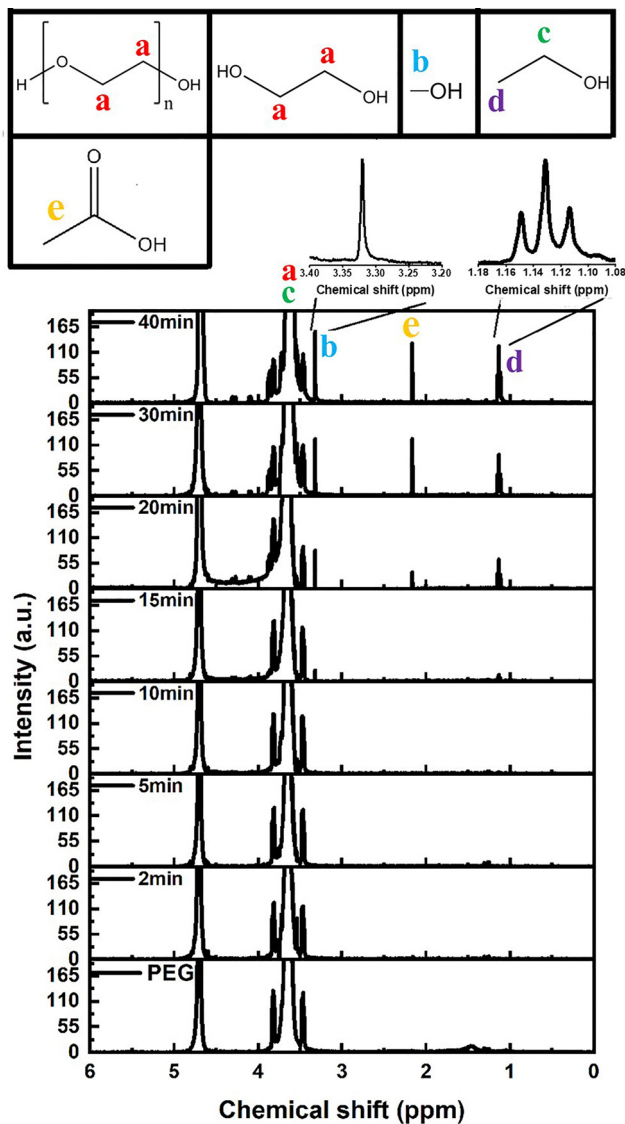


Fig. 4 The effect of reaction time on the  $^1\text{H}$  NMR spectra of liquid products of nonthermal plasma-assisted hydrolysis of PEG.

the PEG structure are broken, leading to liquid products with chain lengths that have more uniform molecular weights compared to the original PEG before hydrolysis reaction.

Fig. S3 shows the zoomed MALDI spectra of PEG and the distance between the main peaks. As shown in this Figure, the difference between  $m/z$  values of every two adjacent main peaks is 44, which is the molar mass of ethylene oxide the monomer from which PEG is formed. This value is the same for all samples before and after the hydrolysis reaction. Therefore, it can be inferred that the bond cleavage can result in the separation of ethylene oxide monomers from PEG chains, resulting in shorter chains. Longer reaction times can break more bonds and release more ethylene oxide, resulting in shorter and lighter PEG chains.

### Reaction pathway and DFT calculations

Non-thermal water plasma produces various reactive species, including hydrogen radicals ( $\cdot\text{H}$ ), hydroxide radicals ( $\cdot\text{OH}$ ),

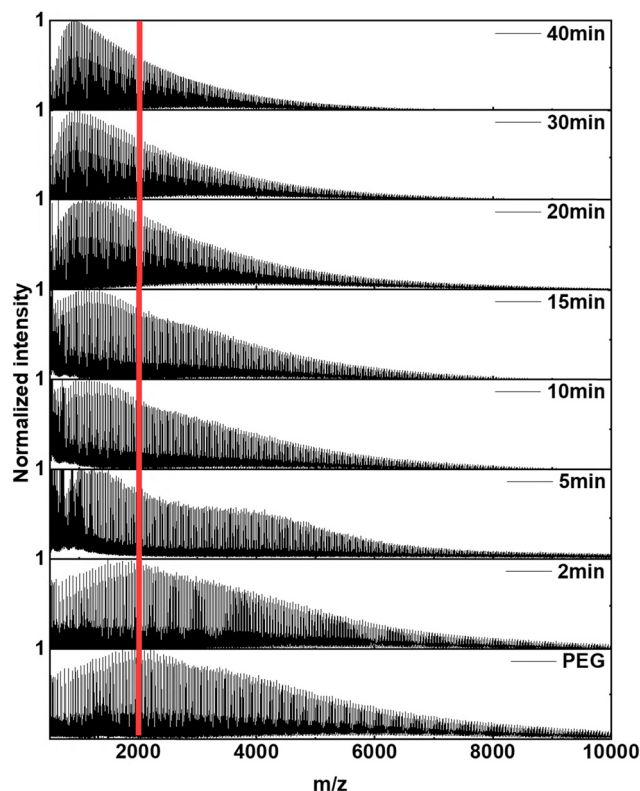


Fig. 5 The effect of reaction time on the MALDI spectra of liquid products of nonthermal plasma-assisted hydrolysis of PEG.

protons ( $\text{H}^+$ ), hydroxide anions ( $\text{OH}^-$ ), atomic oxygen ( $\text{O}$ ), and free electrons, which are considered the main reactive species generated.<sup>42,43</sup> The optical emission spectrum collected during nonthermal water vapor plasma is shown in Fig. S4. Prominent emission features include peaks at 656 nm and 777 nm, corresponding to atomic hydrogen radical ( $\text{H}_\alpha$ ,  $n = 3 \rightarrow n = 2$  transition) and atomic oxygen, respectively, confirming water dissociation.<sup>44,45</sup> Each of these species can potentially react with PEG molecules. This study focuses on the role of  $\cdot\text{OH}$  and  $\cdot\text{H}$  radicals in PEG bond cleavage due to their high reactivity. To explore the reaction pathways, density functional theory (DFT) with the B3LYP/6-31++G(d,p) functional and basis set was employed to investigate possible reactions of a 5-mer PEG molecule in the gas phase. All harmonic frequency calculations were performed at a temperature of 120 °C. While more comprehensive studies are needed to fully understand the reactions of all species, these can be computationally intensive. However, we believe that our current approach and assumptions are reasonable and can contribute to a better understanding of the primary reactions responsible for PEG depolymerization. Since  $\cdot\text{OH}$  and  $\cdot\text{H}$  radicals are assumed to play a significant role in depolymerization, identifying the primary reaction sites in PEG is crucial for proposing the reaction pathway. Previous studies have demonstrated that  $\cdot\text{OH}$  and  $\cdot\text{H}$  radicals can abstract hydrogen or hydroxyl groups from the polymer backbone.<sup>46–49</sup> Therefore, it is valuable to investigate the activation energy for H/OH abstraction at different sites by these radical species. Table S1 presents the

reactions of  $\bullet\text{OH}$  and  $\bullet\text{H}$  radicals with a PEG dimer and their corresponding activation free energies. The results indicate that  $\bullet\text{OH}$  radicals have lower activation free energy than  $\bullet\text{H}$ , suggesting higher activity of hydroxyl. It is also observed that the methyl groups in the middle of the chain are the most likely reaction sites for hydrogen abstraction, as shown in reaction (R1). While most activation energy values are generally below  $5\text{ kcal mol}^{-1}$ , reactions (R5) and (R7) have higher activation energies, making these reactions less likely to occur. Additionally, the formation of water during reactions (R1), (R2), and (R3) can lead to exothermic reactions, whereas the formation of  $\text{H}_2$  has a lower enthalpy of formation.

Based on the activation energies listed in Table S1, potential reaction pathways have been proposed, as illustrated in Fig. 6. Due to its higher reactivity,  $\bullet\text{OH}$  attacks  $-\text{CH}_2$  groups in the PEG chain, abstracts a hydrogen atom, forms water, and creates a  $-\bullet\text{CH}-$  site in the chain. Similarly, hydrogen abstraction can occur with  $\bullet\text{H}$ , leading to the formation of  $\text{H}_2$ . When  $\bullet\text{H}$  interacts with a nearby ether oxygen (highlighted by a blue circle and shown in red), it cleaves the ether bond, breaking the chain into smaller segments. This cleavage is facilitated by the presence of water and the formation of hydrogen bonds with the PEG molecule. Overall, the primary mechanism of PEG depolymerization involves hydrogen abstraction from  $-\text{CH}_2$  groups followed by ether bond cleavage, resulting in shorter PEG chains. DFT calculations show that ether bond cleavage leads to the formation of various end-groups, resulting in multiple species in the liquid phase, as indicated by the green circle. The formation free energy

values for these products are listed in Table S2, with the ethyl-end functional group being the most stable product. The reactions of different end-functional groups with radical species are detailed in Tables S3–S5, as highlighted in the black box. From these reactions, the primary product is ethylene glycol, which is present in all end-functional chains, followed by smaller quantities of ethanol, methanol, formaldehyde, and acetic acid. Fig. 6 depicts these final liquid-phase molecules in red. Additionally, ethylene glycol can convert into methanol and ethanol, with methanol requiring less activation energy for formation than ethanol, as shown in Table S6. Once these small molecules are present in the liquid phase, gas molecules such as  $\text{CH}_4$ ,  $\text{CO}_2$ , and  $\text{CO}$  are expected to form. After methanol and ethanol oxidize (as detailed in Tables S7 and S8) and transform into formaldehyde, acetaldehyde, formic acid, and acetic acid, the formation of  $\text{CH}_4$ ,  $\text{CO}$ , and  $\text{CO}_2$  begins, requiring higher activation energies (over  $60\text{ kcal mol}^{-1}$  for  $\text{CH}_4$  and  $\text{CO}_2$ ), with calculated values presented in Tables S9 and S10.<sup>50,51</sup> It is important to note that acetaldehyde, formaldehyde, and formic acid have much lower boiling points than the system's temperature ( $120\text{ }^\circ\text{C}$ ) and thus become unstable, converting into other species.

The DFT calculation results indicate that the main liquid products are ethylene glycol, ethanol, methanol, and acetic acid, aligning with the NMR findings in Fig. 4. The results also show that gas-phase products, such as  $\text{CH}_4$ ,  $\text{CO}$ , and  $\text{CO}_2$ , primarily form from the reaction of radical species with liquid-phase products. Moreover, higher activation energies may restrict the initial formation of these gas molecules.

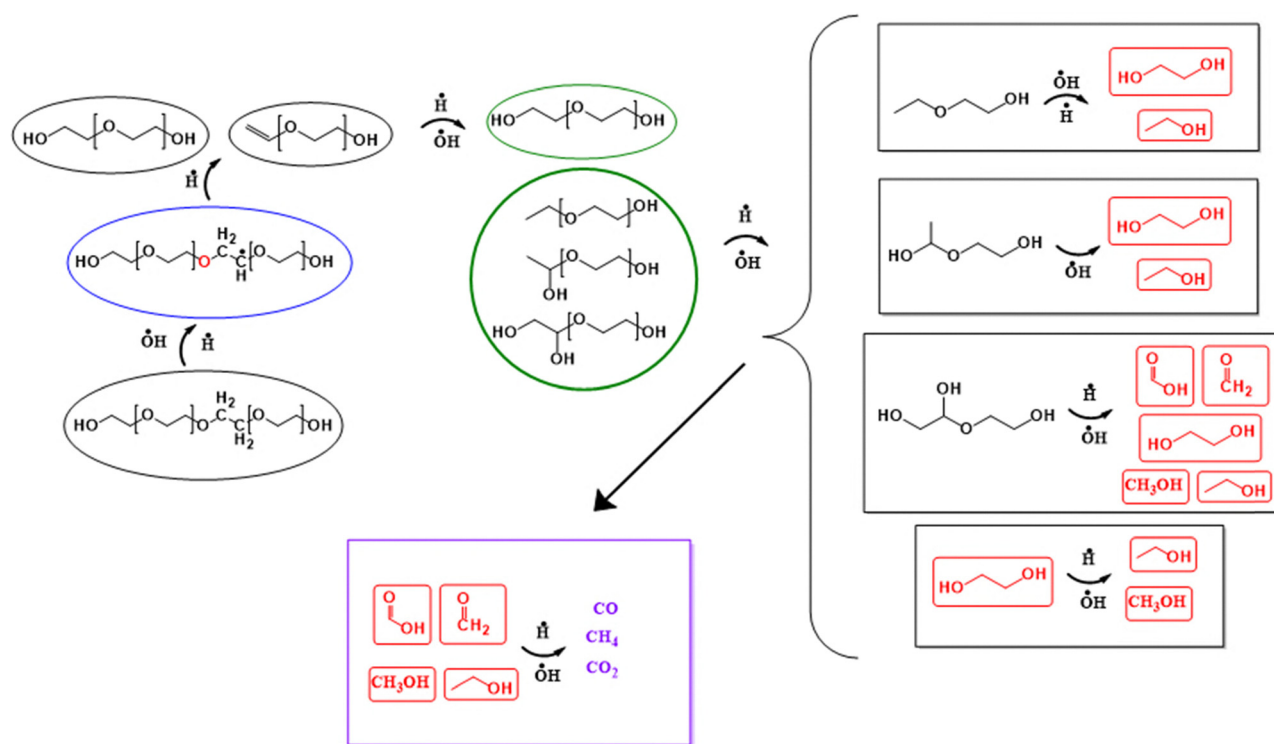


Fig. 6 Computational DFT Pathway to the de-polymerization of hydrolysis PEG. The species in red and purple represent the possible final products in the liquid and gas phases, respectively.



## Conclusions

The findings from the nonthermal plasma-assisted decomposition of PEG in the presence of water vapor show significant advantages over conventional thermal hydrolysis methods, particularly its significantly faster reaction rate. The reaction resulted in the complete conversion of PEG to liquid and gas products, except for the 2-minute reaction where 11 wt% PEG remained unreacted. The time-dependent shift observed in product distribution, from liquid to gas, suggests that secondary reactions within the initial liquid products contribute to further gas production as reaction time increases. Specifically, the gas weight percentage increased from 1.43% at 5 minutes to 12.29% at 40 minutes, reflecting the progressive breakdown of liquid intermediates into gaseous products through bond cleavage. Compounds such as ethanol, methanol, and acetic acid play significant roles in generating gas products, facilitated by interactions with hydroxyl radicals generated from water vapor plasma. Analyses of liquid products *via*  $^1\text{H}$  NMR and MALDI spectra showed significant structural changes in PEG. Notably, shorter PEG chains are formed as reaction time increases, with MALDI showing a significant reduction in  $m/z$  values, from 2000 to 950, confirming bond cleavage within the PEG structure. These changes yield more uniform chain lengths and molecular weights within the liquid products. Based on the proposed reaction pathway and DFT calculations, liquid products, mainly composed of methanol, ethanol, acetic acid, ethylene glycol, and short-chain PEGs start to be produced first as a result of the presence of both  $\bullet\text{OH}$  and  $\bullet\text{H}$  reactive species. Later, gaseous products can be formed as a result of the conversion of the ethanol and methanol, due to their reaction with  $\bullet\text{OH}$ , to the formaldehyde, acetaldehyde, and formic acid which can further interact with  $\bullet\text{OH}$  and  $\bullet\text{H}$  to yield the main gas products including  $\text{CH}_4$ ,  $\text{CO}$ , and  $\text{CO}_2$ . Finally, it should be mentioned that the high energy consumption related to the generation of non-thermal plasma may result in increased costs. Consequently, further investigations should be done to optimize the reaction parameters and conditions, aiming to enhance the energy efficiency of this method.

## Author contributions

Parsa Pishva: investigation, formal analysis, methodology, validation, writing – original draft. Abdol Hadi Mokarizadeh: formal analysis, validation, writing – original draft. Rongxuan Xie: visualization. Jinyao Tang: formal analysis. Xiaochen Shen: investigation. Yanlin Zhu: writing – original draft. Mesfin Tsige: conceptualization, supervision, writing – review & editing. Zhenmeng Peng: conceptualization, supervision, funding acquisition, writing – review & editing.

## Conflicts of interest

There are no conflicts to declare.

## Data availability

The data supporting this article have been included as part the supplementary information (SI) and will be made available upon considerable request. Supplementary information includes gas product mass and FTIR spectra, MALDI analysis of PEG, optical emission spectra of the water vapor nonthermal plasma, and DFT-calculated results. See DOI: <https://doi.org/10.1039/d5ya00163c>.

## Acknowledgements

We acknowledge the financial support of this work by National Science Foundation (2132178).

## References

- 1 E. Otal and J. Lebrato, *J. Chem. Technol. Biotechnol.*, 2003, **78**, 1075–1081.
- 2 D. F. Dwyer and J. M. Tiedjel, *Appl. Environ. Microbiol.*, 1986, **52**, 852–856.
- 3 G. F. White, N. J. Russell and E. C. Tidswell, *Microbiol. Rev.*, 1996, **60**, 216–232.
- 4 D. P. Cox, *Adv. Appl. Microbiol.*, 1978, **23**, 173–194.
- 5 J. R. Haines and M. Alexander, *Appl. Microbiol.*, 1975, **29**, 621–625.
- 6 J. Ulbricht, R. Jordan and R. Luxenhofer, *Biomaterials*, 2014, **35**, 4848–4861.
- 7 G. Liu, Y. Li, L. Yang, Y. Wei, X. Wang, Z. Wang and L. Tao, *RSC Adv.*, 2017, **7**, 18252–18259.
- 8 H. P. Smyth, C. P. Carpenter and C. S. Weil, *J. Am. Pharm. Assoc.*, 1950, **39**, 349–354.
- 9 H. F. Smyth, C. P. Carpenter and C. S. Weil, *J. Am. Pharm. Assoc.*, 1955, **44**, 27–30.
- 10 H. P. Le Khanh, D. Nemes, Á. Ruzsnyák, Z. Ujhelyi, P. Fehér, F. Fenyvesi, J. Várad, M. Vecsernyés and I. Bácskay, *Polymers*, 2022, **14**, 279.
- 11 S. Han, C. Kim and D. Kwon, *Polymer*, 1997, **38**, 317–323.
- 12 J. Glastrup, *Polym. Degrad. Stab.*, 1996, **52**, 217–222.
- 13 L. Yao, J. King, D. Wu, S. S. C. Chuang and Z. Peng, *Catal. Commun.*, 2021, **150**, 106274.
- 14 M. Khatibi, M. A. Nahil and P. T. Williams, *Energy Fuels*, 2024, **38**, 1240–1257.
- 15 I. Aminu, M. A. Nahil and P. T. Williams, *Energy Fuels*, 2022, **36**, 3788–3801.
- 16 Q. Yan, J. Li, J. Zhang and Z. Cai, *Polymers*, 2018, **10**, 729.
- 17 N. Misra, S. Bhatt, F. Arefi-Khonsari and V. Kumar, *Plasma Processes Polym.*, 2021, **18**, 2000215.
- 18 D. Chen, K. Cen, X. Zhuang, Z. Gan, J. Zhou, Y. Zhang and H. Zhang, *Combust. Flame*, 2022, **242**, 112142.
- 19 K. H. Lim, Y. Yue, N. Bella, X. Gao, T. Zhang, F. Hu, S. Das and S. Kawi, *ACS Sustainable Chem. Eng.*, 2023, **11**, 4903–4933.
- 20 S. A. Theofanidis, E. Delikonstantis, V. L. Yfanti, V. V. Galvita, A. A. Lemonidou and K. Van Geem, *Waste Manage.*, 2025, **193**, 155–170.
- 21 H. H. Kim, *Plasma Processes Polym.*, 2004, **1**, 91–110.



- 22 K. H. Baek, D. Jang, T. Kim, S. Ryoo, J.-Y. Yang, J. S. Park, E. Kim and S. Lee, *ACS Appl. Polym. Mater.*, 2022, **4**, 8127–8135.
- 23 F. Li, G. Li, B. G. Lougou, Q. Zhou, B. Jiang and Y. Shuai, *Waste Manage.*, 2024, **189**, 364–388.
- 24 X. Tang, J. Wang, H. Yi, S. Zhao, F. Gao, Y. Huang, R. Zhang and Z. Yang, *Energy Fuels*, 2017, **31**, 13901–13908.
- 25 B. Mehravani, A. I. Ribeiro, U. Cvelbar, J. Padrao and A. Zille, *ACS Appl. Polym. Mater.*, 2022, **4**, 3908–3918.
- 26 P. Pishva, J. Li, R. Xie, J. Tang, P. Nandy, T. Farouk, J. Guo and Z. Peng, *Chem. Eng. J.*, 2024, **501**, 157776.
- 27 S. Y. Liu, D. H. Mei, M. A. Nahil, S. Gadkari, S. Gu, P. T. Williams and X. Tu, *Fuel Process. Technol.*, 2017, **166**, 269–275.
- 28 J. Herzberger, K. Fischer, D. Leibig, M. Bros, R. Thiermann and H. Frey, *J. Am. Chem. Soc.*, 2016, **138**, 9212–9223.
- 29 S. Podaralla, R. Averineni, M. Alqahtani and O. Perumal, *Mol. Pharmaceutics*, 2012, **9**, 2778–2786.
- 30 H. Asadi, K. Rostamizadeh, D. Salari and M. Hamidi, *Int. J. Pharm.*, 2011, **416**, 356–364.
- 31 M. D. Bocharé and M. S. Degani, *ACS Sustainable Chem. Eng.*, 2017, **5**, 3716–3720.
- 32 Q. Li, A. P. Constantinou and T. K. Georgiou, *J. Polym. Sci.*, 2021, **59**, 230–239.
- 33 R. Godelmann, F. Fang, E. Humpfer, B. Schütz, M. Bansbach, H. Schäfer and M. Spraul, *J. Agric. Food Chem.*, 2013, **61**, 5610–5619.
- 34 G. D. Brown, J. Bauer, H. M. I. Osborn and R. Kuemmerle, *ACS Omega*, 2018, **3**, 17957–17975.
- 35 A. Zuriarrain, J. Zuriarrain, A. I. Puertas, M. T. Dueñas and I. Berregi, *Food Control*, 2015, **52**, 49–53.
- 36 I. Jum'h, A. Telfah, J. Lambert, M. Gogiashvili, H. Al-Taani and R. Hergenroder, *J. Mol. Liq.*, 2017, **227**, 106–113.
- 37 G. G. Shimamoto and M. Tubino, *Fuel*, 2016, **175**, 99–104.
- 38 Y. Dong, C. Dai and Z. Lei, *Ind. Eng. Chem. Res.*, 2018, **57**, 11167–11177.
- 39 S. Pandey, *Heat Transfer*, 2022, **51**, 3334–3352.
- 40 A. W. Budiman, J. S. Nam, J. H. Park, R. I. Mukti, T. S. Chang, J. W. Bae and M. J. Choi, *Catal. Surv. Asia*, 2016, **20**, 173–193.
- 41 H. Yue, Y. Zhao, X. Ma and J. Gong, *Chem. Soc. Rev.*, 2012, **41**, 4218–4244.
- 42 N. L. Aleksandrov, E. M. Bazelyan, A. A. Ponomarev and A. Y. Starikovskiy, *J. Phys. D: Appl. Phys.*, 2022, 55.
- 43 Y. Gorbanev, D. O'Connell and V. Chechik, *Chem. – Eur. J.*, 2016, **22**, 3496–3505.
- 44 J. de Oliveira Mallia, S. Griffin, C. Buttigieg and R. Gatt, *Front. Chem.*, 2024, 12.
- 45 P. Amarnath, N. Nandy, B. Indumathy and S. Yugeswaran, *J. CO<sub>2</sub> Util.*, 2022, **66**, 102290.
- 46 D. Jiang, S. Barata-Vallejo, B. T. Golding, C. Ferreri and C. Chatgililoglu, *Org. Biomol. Chem.*, 2012, **10**, 1102–1107.
- 47 K. Fukatsu and S. Kokot, *Polym. Degrad. Stab.*, 2001, **72**, 353–359.
- 48 A. Arts, M. T. de Groot and J. van der Schaaf, *Chem. Eng. J. Adv.*, 2021, **6**, 100093.
- 49 R. Asatryan, Y. Pal, J. Hachmann and E. Ruckenstein, *J. Phys. Chem. A*, 2018, **122**, 9738–9754.
- 50 Y. B. Lim, Y. Tan and B. J. Turpin, *Atmos. Chem. Phys.*, 2013, **13**, 8651–8667.
- 51 F. J. Beltrán, A. M. Chávez, P. Cintas and R. F. Martínez, *J. Phys. Chem. A*, 2023, **127**, 1491–1498.

